Table 1 Comparison of results $M_\infty = 6$, $\gamma = 1.4$

		Int. rel.	Meth. of lines	Inverse[6]
R_B/R_S,	Sphere	0.660	0.677	0.732
	Paraboloid	0.590	0.613	0.662
ϵ,	Sphere	0.148	0.145	0.148
	Paraboloid	0.164	0.158	0.163
χ^*/R_B,	Sphere	0.248	0.234	0.230
	Paraboloid	0.435	0.400	0.479

scheme, the resulting set of equations is conveniently expressed as

$$d\delta/ds = (1 + \delta/R)/\tan(\theta + \chi) \quad (3)$$

$$d\chi/ds = [(F_2 + Qf_1)(d\delta/ds) + F_1]/F_3 \quad (4)$$

$$dV_{S_0}/ds = [F_4 + (F_5 + Qf_2)(d\delta/ds) + F_6(d\chi/ds)]/F_7 = N/D \quad (5)$$

where the $F_i = F_i(s,\delta,\chi,V_{S_0})$ (see Ref. 5) and

$$f_1 = -\tfrac{1}{2}r_1{}^jZ_1, f_2 = \tfrac{1}{2}(r_0{}^jt_0 - r_1{}^jt_1)$$

and $Q = 1$ or 0 for the method of lines or integral relations, respectively.

Reference 5 provides an excellent review of the computational technique. The difference method exhibits the same qualitative behavior as does the integral relations, and consequently the computer program was able to apply the same numerical scheme to both, the only difference being the value of Q in the equations themselves. A Runge-Kutta technique was used to integrate numerically the equations from the axial streamline to the sonic point on the body. A step size of 0.02 was used for all cases; smaller steps were tried with negligible effect on the results. The usual computational problem arises because the equations are elliptic and nominally require that conditions be known along all four boundaries of the strip. Since the shock standoff distance ϵ and the location of the sonic point s^* are not known a priori, a value of ϵ is assumed at the start of each integration and an iterative approach is then followed. In the expression for dV_{S_0}/ds both N and D become identically zero at the sonic point. If the "correct" value of ϵ has been used, the ratio remains well-behaved and finite until $M = 1$ is achieved. However, the slightest deviation from this value (anything above $\sim 10^{-7}$) results in singular behavior of the gradient, and consequently a new ϵ is chosen and the integration begun again at the axis. Note that we treat here only smooth bodies with no discontinuity in slope. If such a "corner" does exist and as is often the case, it is known to coincide with the sonic point, discontinuous behavior in dV_S/ds is to be expected, and the convergence to the appropriate ϵ is greatly simplified.

Typical results are presented in Fig. 2 for both spherical and paraboloidal geometries at $M_\infty = 6$ and $\gamma = 1.4$ in the form of body pressures scaled to twice the freestream dynamic pressure; comparison is made with an inverse scheme by Van Dyke and Gordon.[6] Table 1 gives the corresponding values of shock standoff distance, ratio of body radius to shock radius of curvature at the nose, and location of sonic point on the body.

Other cases have been run for M_∞ ranging from 3–10^4. Generally speaking, the results of both single-strip approximations produce better agreement with the more precise inverse calculations as $M_\infty \to \infty$, which is not surprising in view of the narrowing shock layer. The integral approach is usually slightly more accurate as regards body pressures and detachment distances. As M_∞ enters the hypersonic range, for some geometries the method of lines becomes superior in predicting sonic point location. Since computing the shock radius of curvature involves approximating second-order derivatives, the single-strip methods provide rather poor agreement with Van Dyke's values of R_B/R_S, the method of lines again being closer at high Mach numbers.

In short then, both methods give reasonably good results, each perhaps having a slight advantage in different areas. However, as noted above the application of the method of lines with more than one strip is considerably simpler. In addition, the reluctance toward using it on grounds that many more strips are required to achieve a comparable degree of accuracy is apparently unfounded, at least as concerns the blunt body problem.

References

[1] Belotserkovskii, O. M. and Chuskin, P. I., "The Numerical Method of Integral Relations," *Journal of Computational Mathematics and Mathematical Physics*, Vol. II, No. 5, 1962, pp. 731–759.

[2] Hayes, W. D. and Probstein, R. F., *Hypersonic Flow Theory*, 2nd ed., Academic Press, New York, 1966, Chap. VI, pp. 407–438.

[3] George, A. R., "Perturbations of Plane and Axisymmetric Entropy Layers," *AIAA Journal*, Vol. 5, No. 12, Dec. 1967, pp. 2155–2160.

[4] South, J. C. and Klunker, E. B., "Methods for Calculating Nonlinear Conical Flows," *Analytic Methods in Aircraft Dynamics*, SP-228, NASA, 1969.

[5] Xerikos, J. and Anderson, W. A., "A Critical Study of the Direct Blunt Body Integral Method," Rept. SM-42603, 1962, Missile and Space Systems Div., Douglas Aircraft Co., Santa Monica, Calif.

[6] Van Dyke, M. D. and Gordon, H. D., "Supersonic Flow Past a Family of Blunt Axisymmetric Bodies," TR-R-1, 1959, NASA.

Influence of Initial Flow Direction on the Turbulent Base Pressure in Supersonic Axisymmetric Flow

THOMAS J. MUELLER,* CHARLES R. HALL JR.,† AND PATRICK J. ROACHE‡

University of Notre Dame, Notre Dame, Ind.

Nomenclature

D = diameter
d,j = dividing and separating streamlines in Fig. 2
L,l = afterbody and total body lengths, respectively
M = Mach number
P = absolute pressure
R = reference streamline close to, but outside of, the mixing region

Presented as Paper 70-555 at the AIAA Atmospheric Flight Mechanics Conference, Tullahoma, Tenn., May 13–15, 1970; submitted May 26, 1970; revision received October 5, 1970. Work jointly supported by Air Force Flight Dynamics Laboratory, Air Force System Command, Wright-Patterson Air Force Base, Ohio, under Contract AF-F33615-68-C-1007, NASA under Grant NsG(t)-65, and the Department of Aerospace and Mechanical Engineering.

* Professor. Associate Fellow AIAA.

† Research Assistant. Associate Member AIAA.

‡ NASA Fellow; presently Staff Member, Numerical Fluid Dynamics Division, Sandia Laboratory, Albuquerque, N. M. Member AIAA.

$r,\bar{r}$ = radius and radius of reference system of coordinates, respectively
T = absolute temperature
u = velocity in x or X direction
X,Y = coordinates of the reference (inviscid) coordinate system
x,y = coordinates of the intrinsic (viscous) coordinate system
γ = ratio of specific heats
η = similarity parameter
θ = streamline angle
σ = jet spread parameter
Φ = afterbody angle ($\Phi < 0$ is a boattail; $\Phi > 0$ is a flare)
ϕ = dimensionless velocity defined as u/u_a

Subscripts

a = flow adjacent to the viscous mixing region
b = base
c = cylindrical portion of the body
m = coordinate shift in the mixing theory due to the momentum integral
w = trailing wake
o = stagnation conditions
1–4 = regions shown in Figs. 1 and 2
∞ = freestream conditions

Introduction

THE available axisymmetric base pressure methods assume either a constant or rising pressure along the jet mixing region. References 1–7 considered the development of the jet mixing region to take place only at constant pressure, and Ref. 8, only with rising pressure, but Zumwalt[9,10] and Mueller[11] studied the mixing region with both rising and constant pressure in the direction of flow. The following analysis for the flow over boattails and flares (see Figs. 1 and 2) represents an extension of the rising pressure approach of Ref. 11.

Jet Mixing with Pressure Rise

In the theoretical flow model, the flow is divided into an inviscid freestream, a dissipative mixing layer, and a base region. In addition to using the restricted mixing theory of Korst,[12] the following conditions are imposed on these three flow components: 1) The boundary layer approaching the separation corner is neglected, although the jet mixing is assumed to be fully turbulent. 2) The freestream expands isentropically from 1 to 2; the axisymmetric method of characteristics used for the inviscid flow over the afterbody is continued to the recompression station 3. 3) The conetail surface serves as the "corresponding inviscid jet boundary." Between stations 2 and 3, the pressure normal to the "corresponding inviscid jet boundary" is assumed to be constant within and near the mixing region at each cross section. 4) Velocity profile similarity is assumed in the mixing region. The error function velocity distribution is located within the intrinsic system of coordinates x,y. The coordinate shift between the reference coordinates X,Y and the intrinsic coordinates x,y is represented by $X \simeq x$ and $Y = y - y_m(x)$, where $y_m(0) = 0$. This coordinate shift is a result of using the restricted mixing theory of Korst. 5) The axisymmetric geometry of the mixing region is taken into account in the integral presentation for momentum and mass fluxes between sections 2 and 3. and 6) Recompression is assumed to result from an oblique shock turn from 3 to 4 at the empirically determined trailing wake radius $r_3 \simeq r_w$ (which is based on values for cylindrical bodies[13] for reasons discussed later).

A streamline j in Fig. 2 divides the mass flow passing over the corner at 1 from that entrained by the viscous action of the free jet mixing region. At 3, a streamline d represents flow with just sufficient kinetic energy to negotiate the pressure rise to 4. Streamlines below the d streamline have lower kinetic energies and are turned back to recirculate in the base region. If there is no secondary flow, i.e., no mass bleed into or out of the base region, the conservation of mass requires that the j and d streamlines be identical.

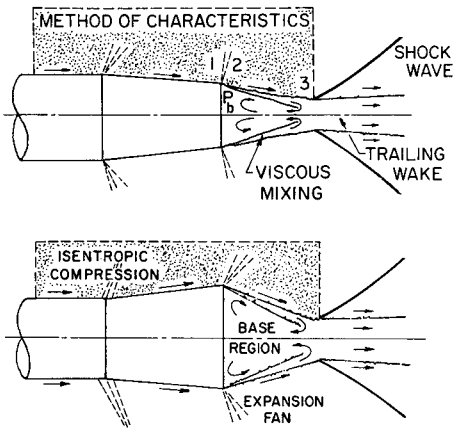

Fig. 1 Essential features of the flow behind axisymmetric conical boattails and flares.

The control volume utilized in the formulation of the equations for conservation of mass and momentum between cross sections 2 and 3 is bounded by streamlines R and $-R$. For the simplified axisymmetric flow model previously described, Zumwalt formulated the momentum equation in the axial direction, using geometrical relations and the relation between the inviscid and viscid coordinate systems. This equation was solved simultaneously with the combined viscid and inviscid continuity equations written for the control volume. For the error function velocity profile $\phi = \frac{1}{2}(1+\text{erf}\ \eta)$ where $\phi = u/u_a$ and $\eta = \sigma y/x$, it was found that $\eta_R = 3$ was large enough for ϕ_j to approach its asymptotic value. The result of this analysis is a nolinear equation which allows one to locate the j streamline at 3. (See Refs. 9–11, 14 and 15 for details of the analysis).

To determine η_{j3} for a given initial condition, we must know the location of the recompression region $\bar{r}_3/r_b$, the corresponding inviscid condition M_{3a}, and the jet spread parameter σ_{3a}. We determine $\bar{r}_3/r_b$ from experimental data for r_w/r_b cited in Ref. 13 for cylindrical bodies in air (Fig. 3). Unfortunately, the effect of initial flow direction on r_w/r_b does not appear to have been published in the open literature. One schlieren photograph was found of the wake behind a boattailed body of revolution at zero angle of attack.[16] The r_w/r_b obtained from this photograph is shown on Fig. 3 and is somewhat higher than the data for flow past a cylindrical body at the same Mach number. The only difference in the calculation procedure from that used in Ref. 11 is that the Mach number along the inviscid jet boundary from 2 to 3, M_{3a}, is determined from the axisymmetric characteristics solution. The jet spread parameter σ_{3a} is determined from the equation obtained by Channapragada.[17]

A FORTRAN IV program for the UNIVAC 1107 digital computer was developed to calculate the axisymmetric flow-

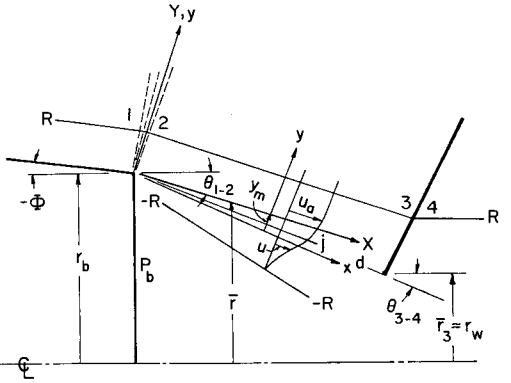

Fig. 2 Flow model for the influence of initial flow direction on the axisymmetric turbulent base pressure.

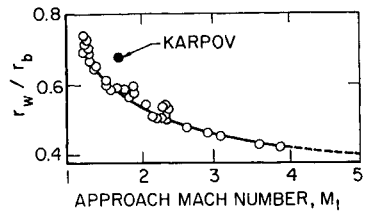

Fig. 3 Trailing wake radius ratio vs Mach number for $\gamma = 1.4$.[13]

field over conical boattailed and flared bodies of revoltuion using the axisymmetric method of characteristics. It yields the necessary initial flow field for the base pressure determination, which forms the second part of the total computer program, that is detailed in Ref. 14. The separation criterion given by Zukoski[18] is included in the program in order to indicate the possibility of separation on boattailed afterbodies.

Results for Conical Afterbodies

References 16 and 19–25 provide experimental afterbody and base pressure data for bodies of revolution with conical, circular arc, and parabolic boattails for various M_∞'s from 1.7 to 6.0. Because of the possible occurrence of flow separation, as well as interference by the model suport, these data must be examined carefully before comparisons can be made with the analytical results. At this point, the conical boattail data of Refs. 21 and 25 appear to be the most promising for the present study.

Fig. 4 shows excellent agreement between the analytical results for $\gamma = 1.4$, $T_b/T_{oa} = 1$, $M_c = 2.0$, and $r_b/r_c = 0.58$, and the experimental data of Reid and Hastings,[21] for cases of uniform external flow except for a relatively thin turbulent boundary layer. (Other data available either include nose effects, angle-of-attack effects, and/or undetermined boundary-layer character and thickness approaching the base.) For small angles (i.e., $|\Phi| < 3°$) and moderate r_b/r_c, L becomes large, requiring a large grid size. However, if the curve of Fig. 4 is extrapolated to $\Phi = 0$, the resulting P_b/P_1 agrees with that for the flow over a cylindrical body obtained by Mueller,[11] i.e., $P_b/P_1 \simeq 0.60$.

Reference 25 gave P_b (M_∞) for the bodies of revolution shown in Fig. 5. While the influence of initial boundary layer would not be expected to be large for these short bodies, use of the assumption of uniform Mach number and flow direction in the inviscid flow ahead of the boattail is not obvious for these geometries. These questions would be resolved by computing the entire flowfield (inviscid and viscid) about this type of body. The theoretical results in Fig. 5 were obtained by neglecting the initial boundary layer and assuming a uniform flow ahead of the boattail. The theory correctly predicts the influence of M_∞ on P_b/P_∞, but the calculated values of P_b/P_∞ are consistently lower than the experimental data by 6% to 16%. It is well-known that the presence of an initial boundary layer increases P_b/P_∞; thus, inclusion of the initial boundary layer in the analysis would bring the results closer

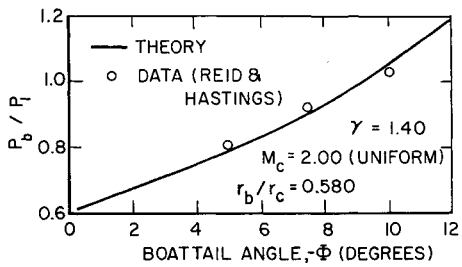

Fig. 4 Comparison of theory with data of Ref. 21 for the influence of boattail angle on the base pressure ratio for conical boattails and uniform initial flow.

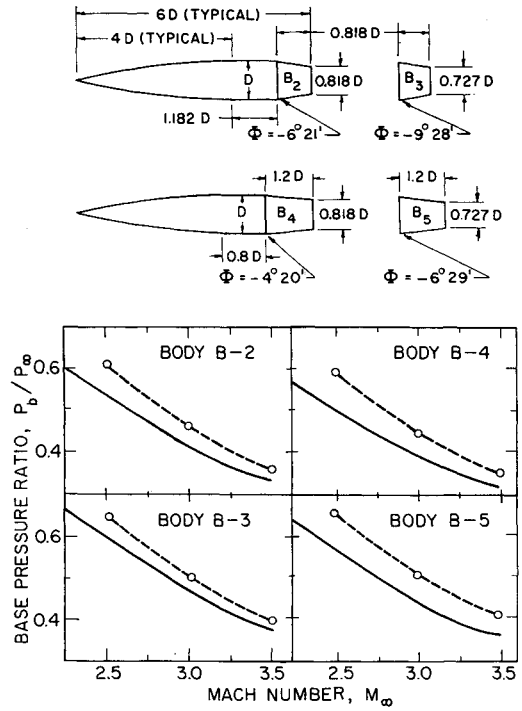

Fig. 5 Comparison of theory (solid curves) with data of Ref. 25, assuming uniform flow ahead of boattail.

to the experimental data. Including the nonuniform character of the inviscid flow may also improve the agreement.

A somewhat small number of experiments appear to have been performed on bodies of revolution with flares (e.g., Refs. 26–28), and most of them included extensive regions of flow separation and/or did not include determinations of P_b. An attempt was made to compare the present analytical method with some of the data presented in Ref. 28 for blunt-nosed bodies (Fig. 6). The Mach number at the beginning of the flare was assumed to be uniform and was obtained from the pressure ratio data of Ref. 28. Although the theory pre-

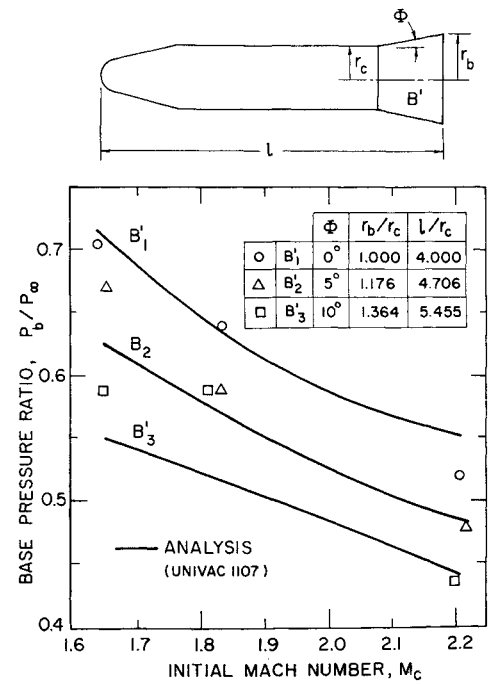

		Φ	r_b/r_c	l/r_c
○	B'_1	0°	1.000	4.000
△	B'_2	5°	1.176	4.706
□	B'_3	10°	1.364	5.455

Fig. 6 Influence of Mach number on base pressure ratio for blunt-nosed bodies with conical flares, assuming uniform flow ahead of flare.[28]

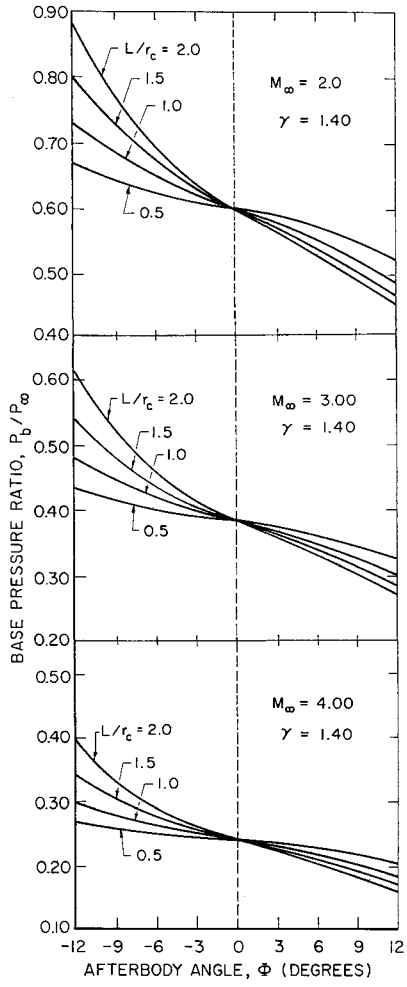

Fig. 7 Theoretical influence of afterbody angle and length on the base pressure ratio for conical afterbodies $T_b/T_{oa} = 1$.

dicts the trends of the experimental data reasonably well, it is apparent that a more complete set of data is needed to evaluate the analysis for flared bodies.

Figure 7 presents the predicted effects of Φ and L/r for three M_∞'s (equal to uniform M_c's) for $\gamma = 1.4$ and $T_b/T_{oa} = 1$. As $\Phi \rightarrow 0$ from either direction, the well established P_b/P_∞ for a cylindrical body is reached. This parametric presentation should be of value to vehicle designers. In accord with the foregoing discussion, the results for conical boattails ($\Phi < 0$) are the more reliable at present. It is believed that the analytical method can be applied to any afterbody shape and can be extended to include the effects of mass bleed, initial boundary layer, nonisoenergetic jet mixing, and the ratio of specific heats.

References

[1] Korst, H. H., Zumwalt, G. W., and Chow, W. L., "Research on Transonic and Supersonic Flow of a Real Fluid at Abrupt Increases in Cross Section," ME-TN-392-5, OSR-TR-60-74, Dec. 1959, University of Illinois, Urbana, Ill.

[2] Beheim, M. A., "Flow in the Base Region of Axisymmetric and Two-Dimensional Configurations," TR R-77, 1961, NASA.

[3] Minyatov, A. V., "Raschet donnogo davleniya v sverkhzvukovom potoke obtekayushchem telo vrascheniya (Calculation of the Base Pressure in the Supersonic Flow About a Body of Revolution)," *Mekhanika i Mashinostroenie*, Izvestiya Akademii Nauk U.S.S.R., Otdelenie Tekhnicheskikh Nauk, No. 3, May–June 1961, pp. 32–39.

[4] Tagirov, R. K., "Determination of the Base Pressure and the Base Temperature Following the Sudden Expansion of a Sonic or Supersonic Stream," *Mekhanika i Mashinostroenie*, Izvestia Akademii Nauk U.S.S.R., Otdelenie Tekhnicheskikh Nauk, No. 5, Sept.-Oct. 1961, pp. 30–37.

[5] McDonald, H., "An Analysis of the Turbulent Base Pressure Problem in Supersonic Axisymmetric Flow," Rept. Ae. 200, April 1964, British Aircraft Corp., Preston Division, Lancashire, England.

[6] McDonald, H., "An Analysis of the Turbulent Base Pressure Problem in Supersonic Axisymmetric Flow," *The Aeronautical Quarterly*, Vol. 16, May 1965.

[7] Przirembel, C. E. G. and Page, R. H., "Analysis of Axisymmetric Supersonic Turbulent Base Flow," presented at the 1968 Heat Transfer and Fluid Mechanics Institute, June 1968, University of Washington, Seattle, Wash.

[8] Vereshchagina, L. I., "On the Base Pressure for Solids of Revolution in a Supersonic Gas Flow," *Herald of Leningrad University*, Issue 3, No. 13, pp. 208–214; also STAR N66-17406 08-23.

[9] Zumwalt, G. W., "Analytical and Experimental Study of the Axially-symmetric Supersonic Base Pressure Problem," PhD dissertation, 1959, Department of Mechanical Engineering, University of Illinois, Urbana, Ill.; also MIC 59-4589, University Microfilms, Inc., Ann Arbor, Mich.

[10] Zumwalt, G. W. and Tang, H. H., "Transient Base Pressure Study of an Axisymmetric Supersonic Missile Flying Head-on Through a Blast Wave," Research Rept SBW-6, Feb. 1964, School of Mechanical Engineering, Oklahoma State University, Stillwater, Okla.

[11] Mueller, T. J., "Determination of the Turbulent Base Pressure in Supersonic Axisymmetric Flow," *Journal of Spacecraft and Rockets*, Vol. 5, No. 1, Jan. 1968, pp. 101–107.

[12] Korst, H. H., "A Theory for Base Pressures in Transonic and Supersonic Flow," *Journal of Applied Mechanics*, Vol. 23, No. 4, Dec. 1956, pp. 593–600.

[13] Chapman, D. R., "An Analysis of Base Pressure at Supersonic Velocities and Comparison with Experiment," Rept. 1051, 1951, NACA (supercedes TN-2137, 1950, NACA).

[14] Mueller, T. J. and Hall, C. R., Jr., "Analytical Prediction of the Turbulent Base Pressure in Supersonic Axisymmetric Flow Including the Effect of Initial Flow Direction," AFFDL-TR-68-132, Sept. 1968, Air Force Flight Dynamics Lab., Wright-Patterson Air Force Base, Ohio.

[15] Mueller, T. J., Hall, C. R., Jr., and Roache, P. J., "The Influence of Initial Flow Direction on the Turbulent Base Pressure in Supersonic Axisymmetric Flow," AIAA Paper No. 70-555, Manchester, Tenn., 1970.

[16] Karpov, B. G., "The Effect of Various Boattail Shapes on Base Pressure and Other Aerodynamic Characteristics of a 7-Caliber Long Body of Revolution at M = 1.70," Rept. 1295, Aug. 1965, Ballistics Research Lab., Aberdeen, Md.

[17] Channapragada, R. S., "Compressible Jet Spread Parameter for Mixing Zone Analyses," *AIAA Journal*, Vol. 1, No. 9, Sept. 1963, pp. 2188–2189.

[18] Zukoski, E. E., "Turbulent Boundary-Layer Separation in Front of a Forward-Facing Step," *AIAA Journal*, Vol. 5, No. 10, Oct. 1967, pp. 1746–1753.

[19] Cortright, E. M., Jr. and Schroeder, A. H., "Investigation at Mach Number 1.91 of Side and Base Pressure Distribution Over Conical Boattails Without and With Jet Flow Issuing from Base," RM E51F27, 1951, NACA.

[20] Reller, J. O., Jr. and Hamaker, F. M., "An Experimental Investigation of the Base Pressure Characteristics of Nonlifting Bodies of Revolution at Mach Numbers from 2.73 to 4.98," TN 3393, March 1955, NACA.

[21] Reid, J. and Hastings, R. C., "Experiments on the Axi-Symmetric Flow Over Afterbodies and Bases at M = 2.0." Rept. 2628, Oct., 1959, Royal Aircraft Establishment, Farnborough, England.

[22] Brazzel, C. E., "The Effects of Base Bleed and Sustainer Rocket Nozzle Diameter and Location on the Base Drag of a Body of Revolution with Concentric Boost and Sustainer Rocket Nozzles," Rept. RF-TR-63-23, July 15, 1963, U.S. Army Missile Command, Redstone Arsenal, Ala.

[23] Staylor, W. F. and Goldberg, T. J., "Afterbody Pressures on Boattailed Bodies of Revolution Having Turbulent Boundary Layers at Mach 6," TN D-2761, May 1965, NASA.

[24] Brazzel, C. E. and Henderson, J. H., "A Correlation of the Base Drag of Bodies-of-Revolution with a Jet Exhausting Through the Base," AD 634 662, U.S. Army Missile Command, Redstone Arsenal, Ala.

[25] Brazzel, C. E., unpublished data, 1967, U.S. Army Missile Command, Redstone Arsenal, Ala.

[26] Becker, J. V. and Korycinski, P. F., "Heat Transfer and Pressure Distribution at Mach Number of 6.8 on Bodies with Conical Flares and Extensive Flow Separation," TN D-1260, April 1962, NASA.

[27] Goldberg, T. J., "Turbulent Separation Associated with Axisymmetric Flared Bodies," *Journal of Spacecraft and Rockets*, Vol. 4, No. 11, Nov. 1967, pp. 1551–1553.

[28] Henderson, J. H., "Jet Effects on Base Pressures of Cylindrical and Flared Afterbodies at Free-Stream Mach Numbers of 1.65, 1.82 and 2.21," ARGMA TR 1G3R, June 1960; U.S. Army Ordnance Missile Command, Redstone Arsenal, Ala., classification change to unclassified March 21, 1961.

A Method for More Reproducible Burning Rate Determination

W. T. Brooks*
Rocketdyne/North American Rockwell Corporation, McGregor, Texas

Nomenclature

A_b	=	burning surface area
A_t	=	nozzle throat area
a	=	constant in burning rate equation
c^*	=	characteristic exhaust velocity
g_c	=	gravitational conversion constant
n	=	pressure exponent
P	=	pressure
r,r'	=	burning rate, Eqs. (1) and (4), respectively
t_b	=	burning time
W_p,w	=	propellant weight and web thickness, respectively
ρ_p	=	propellant density
σ,σ'	=	standard deviations for r and r', respectively

Introduction

CONVENTIONAL methods for calculating burning rate from a solid propellant motor test firing rely on measured values of burning duration and propellant web distance. A simple manual method is given here with supporting data which provides in many cases a more reproducible burning rate for sliverless motors. It is relatively insensitive to selection of the aft tangent point, and has particular application to burning rate reduction from laboratory scale motors.

Discussion

Burning rate is typically defined by

$$r = w/t_b \tag{1}$$

The web (w) is a straightforward measure. Burning time (t_b) is measured from the pressure- or thrust-time record. Customarily, it is defined to be the interval ending when pressure begins to drop rapidly before going into tailoff. Mathematically, this occurs when $d^2p/dt^2 = 0$. Graphically, it may be determined by the widely used method of bisecting the angle between tangents to the pressure-time [$P(t)$] curve on either side of the point where the third derivative vanishes. In either event, impulse delivered beyond this point is variable, and the magnitude of measured burning time as well as tailoff impulse significantly influences the calculated burning rate.

The method considers burning rate from the simplified pressure equation

$$\bar{P} = \bar{A}_b \rho_p c^* r / g_c A_t \tag{2}$$

It should be noted that average pressure from the $P(t)$ curve may not be identical to $\bar{P}$ in Eq. (2) for non-neutral traces.[1] The same can be said for a comparison of the burning rates (r) given in Eqs. (1) and (2).[2] These effects are small, however, and the $P(t)$ traces considered here are reasonably neutral burning.

If the values of c^* and ρ_p in Eq. (2) are replaced by

$$c^* = g_c A_t \int P dt / W_p \text{ and } \rho_p = W_p / \bar{A}_b w \tag{3}$$

burning rate becomes

$$r' = w\bar{P} / \int P dt \tag{4}$$

where the integrals are taken over the total duration.

Equation (4) is equivalent to the ratio of web and time, where

$$t = \int P dt / \bar{P} \tag{5}$$

This was defined as effective time in Ref. 3. Average pressure ($\bar{P}$) is taken to be the average over burning time ending at the aft tangent point. Although assessment of the aft tangent time is necessary in both Eqs. (1) and (4), the magnitude of $\bar{P}$ in Eq. (4) is much less sensitive than t_b in Eq. (1) to the procedure for determining the end of burning time.

Considering a typical subscale test motor with a neutral internal burning tube, Eq. (1) gives the most accurate results from tests yielding the least amount of impulse in the tailoff. Influence of this variable (tailoff impulse) on Eq. (1) should be recognized in assessing the accuracy of the method as well as the burning rate where sliverless grains are used. For example, two aft tangent point selections on the $P(t)$ trace from two independent analyses, one at t_1 and one at $t_1 + \Delta t$, will define burning rates from Eq. (1) which differ by the fraction $(t_1 + \Delta t)/t_1$. Average pressures in Eq. (4) over the two intervals differ by an amount much less than the same fraction. Therefore, the burning rate determined by Eq. (4) is better defined than the burning rate by Eq. (1). In the case where no tailoff exists, Eqs. (4) and (1) are the same. Otherwise, $r' < r$.

Data and Results

The method has been evaluated over a range of burning rate from 0.3 to 0.8 in./sec in a 2-in. motor with carboxy-terminated polybutadiene (CTPB) aluminized propellant. The 2-in. motor has an internal burning tube with outer diameter

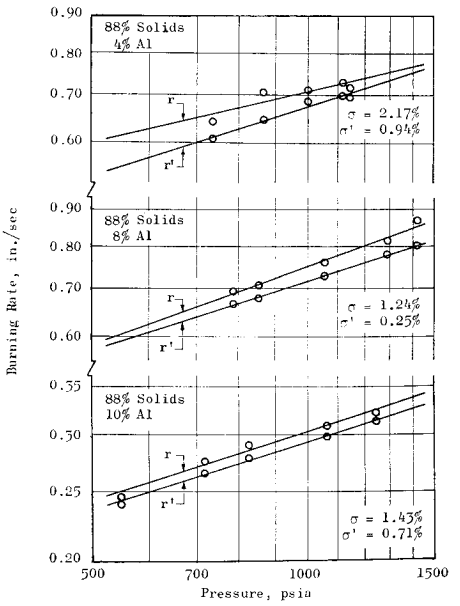

Fig. 1 Comparison of burning rate methods for 3 propellants.

Received July 30, 1970; revision received September 28, 1970.
* Member of the Technical Staff. Associate Fellow AIAA.